Phys. Status Solidi B **252,** No. 7, 1631–1639 (2015) / **DOI** 10.1002/pssb.201451715

physica status solidi b
www.pss-b.com
basic solid state physics

Low-kinetic energy impact response of auxetic and conventional open-cell polyurethane foams

T. Allen[1,2], J. Shepherd[1,3], T. A. M. Hewage[4], T. Senior[1], L. Foster[1], and A. Alderson[*,4]

[1] Centre for Sports Engineering Research, Sheffield Hallam University, Howard Street, Sheffield S1 1WB, UK
[2] Department of Engineering and Mathematics, City Campus, Sheffield Hallam University, Howard Street, Sheffield S1 1WB, UK
[3] SABEL Labs, School of Engineering, Nathan Campus, Griffith University, 170 Kessels Road, Nathan, QLD 4111, Australia
[4] Materials and Engineering Research Institute, Sheffield Hallam University, Howard Street, Sheffield S1 1WB, UK

Received 28 November 2014, revised 25 March 2015, accepted 7 April 2015
Published online 29 April 2015

Keywords auxetic, foam, impact, negative Poisson's ratio

[*] Corresponding author: e-mail aldersonandy@gmail.com, Phone: 0044 114 225 3523, Fax: 0044 114 225 3501

This paper reports quasi-static and low-kinetic energy impact testing of auxetic and conventional open-cell polyurethane foams. The auxetic foams were fabricated using the established thermo-mechanical process originally developed by Lakes. Converted foams were subject to compression along each dimension to 85% and 70% of the unconverted dimension during the conversion process, corresponding to linear compression ratios of 0.85 and 0.7, respectively. The 0.7 linear compression ratio foams were confirmed to have a re-entrant foam cell structure and to be auxetic. Impact tests were performed for kinetic energies up to 4 J using an instrumented drop rig and high speed video. A flat dropper was employed on isolated foams, and a hemispherical-shaped dropper on foams covered with a rigid polypropylene outer shell layer. The flat dropper tests provide data on the rate dependency of the Poisson's ratio in these foam test specimens. The foam Poisson's ratios were found to be unaffected by the strain rate for the impact energies considered here. Acceleration-time data are reported along with deformation images from the video footage. The auxetic samples displayed a six times reduction in peak acceleration, showing potential in impact protector devices such as shin or thigh protectors in sports equipment applications.

1 Introduction Protective sporting equipment can prevent acute injuries [1, 2] and be cost effective when compared to direct medical costs [3]. For the equipment to be effective, injury mechanisms, load ranges, human tolerances and material performances all need to be understood [4]. Protective equipment usually performs impact energy attenuation, acceleration management, load distribution and force limitation. Foams often serve as the energy absorbing component, while a shell can be utilised to enable more foam to be compressed for a given impact [5–7]. Often the materials used are effective in general use but not for the range of impacts which can occur throughout the sport.

Sanami et al. [8] present a case for applying auxetic foams to protective sporting equipment. Auxetic materials have a negative Poisson's ratio, when placed under compression in one direction they become thinner in one or more perpendicular directions [9]. The general mechanism of obtaining auxetic foam from conventional foam consists of three steps: (i) compression of foam, (ii) softening it to release stress at the compressed state and (iii) stiffening the densified but already unstressed foam. The traditional approach is to use a thermo-mechanical process [10], although a chemo-mechanical process can also be applied [11]. Auxetic foams have some interesting mechanical properties including, synclastic curvature and improved resilience [10], indentation resistance [12, 13], shear resistance [14], fracture toughness [14], energy dissipation [12, 15] and vibration damping [16, 17]. In certain density regions, auxetic foams and isotropic auxetic continua can also display negative bulk modulus [18, 19] and negative compliance [20, 21].

Impact and indentation investigations have previously been reported on auxetic polymeric [22–27] and metallic [12] foams, sandwich panels comprising kevlar fabric-epoxy honeycomb core and fibre-reinforced polymer skins [28], carbon fibre-reinforced epoxy laminates [29],

polymers containing auxetic chopped fibres [30] and microporous polymers [31]. A number of theoretical treatments are also present in the literature [32–37].

Under impact loading, auxetic materials have been shown to offer increased energy absorption [12, 22, 23, 25, 28, 30], higher impact resistance [28–30, 31, 33, 34] and reduced damage area [28–30]. The impact resistance appears to be rate dependent in carbon-epoxy laminates [29], and auxetics appear to be more prone to surface failure under quasi-static and low velocity impact [25, 32], although this is mitigated when a surface layer is placed over the auxetic material [32].

Auxetics have been reported to display higher maximum deceleration during impact [23], which would be expected to lead to increased pressure and, therefore, be detrimental for cushioning applications. However, this is contrary to the measurement of lower maximum seating pressure [26] and an analytical approach [35] which shows negative Poisson's ratio cushions reduce the peak pressure if the cushion shear modulus is held constant as Poisson's ratio is varied. In the case of the cushion Young's modulus being held constant, Wang and Lakes show that the optimal Poisson's ratio is zero. Auxetic materials have been suggested to offer the best solution for reducing impact forces which may be distributed over a wide area (e.g. person's back) or a narrow area (e.g. elbow) in, for example, wrestling mat or knee pad applications [33].

Sanami et al. [8] applied the thermo-mechanical process to open-cell polyurethane foam, reporting a reduction in Poisson's ratio from 0.36 to −0.22. Their conventional foams exhibited classical behaviour under quasi-static compression, the stress–strain curve was linear until ∼5% strain and then entered a plateau region [38]. In agreement with Lakes [10], the auxetic foam showed higher resilience, Young's modulus was initially only 15 kPa in comparison to 35 kPa for the conventional foam, but the stress–strain curve showed an extended region of linear elasticity up to maximum compression at 15% strain. Their auxetic foams also absorbed more than double the energy than their conventional counterparts under quasi-static indentation with a sphere. Increased resilience [27, 39] has also been observed in auxetic open-cell polyurethane foams at high compressive strain rates. The effect of strain rate on the strain-dependent negative Poisson's ratios in auxetic foams has also been investigated [39]. Several different foam types were considered and no universal trend with strain rate was observed in response to strain rates up to $9\,s^{-1}$.

Standards for protective sporting equipment usually include an impact test/s, with the pass criterion based on the ability to keep accelerations or transmitted forces below a specified level (e.g. BS 6183-1:1981). The literature on auxetic foams indicates that they have the potential to be applied to produce protective equipment with superior energy absorption and/or reduced thickness. Further work is required to determine the ability of auxetic foams to attenuate impact forces and/or accelerations, to investigate the rate dependency of the auxetic property on impact response, and to establish the effect of a semi-rigid surface layer on the impact response of the auxetic foam. The aim of this paper is to investigate these issues by determining the impact performance of auxetic open-cell polyurethane foam. The findings will be discussed in relation to the application of auxetic foam to protective sporting equipment.

2 Methods This research focussed on quasi-static and low-kinetic energy impact testing to characterise auxetic foams – fabricated with the thermo-mechanical conversion process – in comparison to their conventional counterparts. Through thickness images of the cell structure of the foams were also obtained using a camera (Canon EOS 5D Mark II with EF100mm f/2.8L Macro IS USM lens) on manual exposure. Impact testing was performed with foams in isolation and foams covered with a polypropylene sheet to replicate protective sporting equipment. Performance was based on the ability of the foams to attenuate impact acceleration.

Table 1 shows the materials used, the foams were reticulated open-cell polyurethane, designated by R30FR with 30 pores in^{-1}, R45FR with 45 pores in^{-1} and R60FR with 60 pores in^{-1} (Custom Foams). R45FR corresponds to the foam utilised by Sanami et al. [8] and the unconverted foams had similar densities to those investigated by other authors [27, 39]. Association football shin guards often utilise ethylene vinyl acetate copolymer foams with densities of around 70–100 kgm^{-3} [5], and the conversion process used here resulted in foams with densities within this range. The foam samples tested had dimensions of $75 \times 75 \times 20$ mm and the polypropylene sheets (Direct Plastics, PPH/PP-DWST-Homopolymer) had dimensions of $75 \times 75 \times 1$ mm. The thickness of the foam samples was representative of typical protective sporting equipment. The unconverted foam test samples were cut to size from a monolith.

Table 1 Materials used in this research.

sample type	density ($kg\,m^{-3}$)	number
conventional foam: R30FR, R45FR & R60FR	26–32	15 of each
converted foam with LCR of 0.85: R30FR, R45FR & R60FR	42–52	15 of each
converted foam with LCR of 0.7: R30FR, R45FR & R60FR	76–94	15 of each
polypropylene sheet	905	15

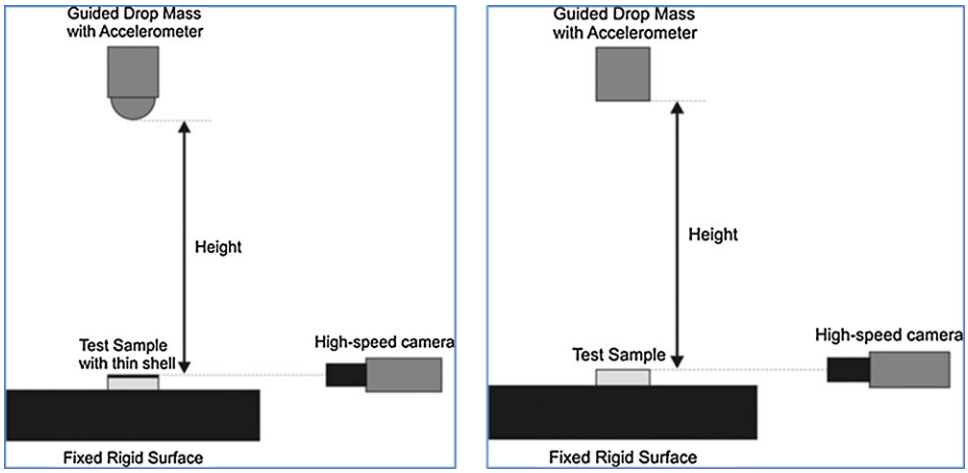

Figure 1 Experimental setup for impact testing consisting of a bespoke instrumented drop rig and high speed camera, (a) hemispherical dropper and (b) flat dropper. The diameter of the hemispherical dropper corresponded to the value specified in the standard for protective equipment for cricketers (BS 6183-1:1981).

To facilitate the thermo-mechanical conversion process, samples exceeding the test dimensions were cut from a monolith. These samples were $118 \times 118 \times 118$ mm for a Linear Compression Ratio (LCR) of 0.85 and $143 \times 143 \times 143$ mm for a LCR of 0.7. LCR is defined as the ratio of the compressed to initial dimensions. The foams were placed inside a compression mould of size $100 \times 100 \times 100$ mm to achieve a triaxial compression, with lubricant applied to reduce edge creasing. The mould containing the compressed foam was placed in an oven at 200 °C. After 30 min, the mould was removed from the oven and the foam was taken from the mould and stretched gently by hand in each of the three directions at room temperature to avoid adhesion of the cell ribs. The foam was reinserted into the mould and placed back into the oven at 200 °C for a further 30 min. The process was repeated for a final time with the oven temperature reduced to 100 °C for 30 min.

Quasi-static compression tests were performed on three samples of each material in a uniaxial test machine (Instron 3369, fitted with a 50 kN load cell). The samples were compressed to 50% strain at a rate of 10 mm min^{-1}, with load and extension recorded at 10 Hz. Young's moduli were obtained from linear regression up to 5% compressive strain, which is within the region of linear elasticity [8, 38].

Low-kinetic energy impact tests were performed using a bespoke drop rig (Fig. 1). A cylindrical flat-faced dropper (2.27 kg and 115 mm diameter face) was employed on foams in isolation and a hemispherical faced dropper (2.09 kg and 73 mm diameter hemisphere) was employed when the foams were covered with the polypropylene sheet. The flat dropper applied a distributed load to the entire face of the sample, while the hemispherical dropper applied a concentrated load at the centre of each composite (foam plus sheet) sample. The sheet was sufficiently thin to provide intermediate behaviour between a concentrated load and an evenly distributed load, as shown in Fig. 2. Drop heights were set at 0.1 and 0.2 m for the flat dropper and 0.1 m for the hemispherical dropper, providing impact energies of ~2 and ~4 J. The dropper was fitted with a wireless accelerometer (PCB, ICP Shock Sensor, 350B24) recording at 50,000 Hz, providing acceleration-time data for each impact (DTS SLICEWare Version 1.08.0475). Five samples of each material were tested in each of the three scenarios, requiring 15 samples of each material.

Poisson's ratios were obtained from the quasi-static tests and flat-faced dropper impact tests. Measurements of Poisson's ratio were not obtained for the hemispherical

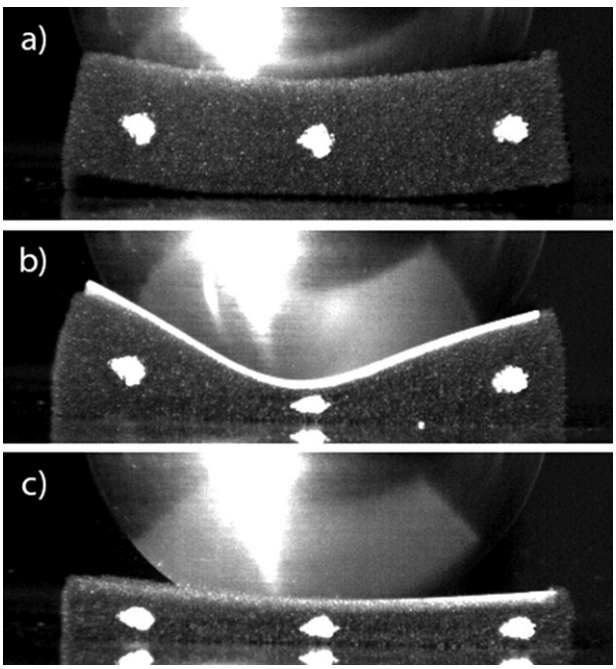

Figure 2 Maximum deformation of the hemispherical dropper on conventional R60FR foam with (a) no sheet, (b) 1 mm thick sheet and (c) 2 mm thick sheet.

dropper tests because the load was not evenly distributed. The quasi-static tests were filmed with a network camera (Axis P1357) at 25 Hz, with a resolution of 1080×720 pixels and the impact tests were filmed with a high-speed camera (Vision Research, Phantom V4.3) at 10,000 Hz, with a resolution of 416×128 pixels and exposure time of 97 μs. The video footage was used to locate temporal centre positions of four marks applied to the front face of each sample, using a bespoke tracking software utilising MATLAB (MathWorks). True strains were calculated in both directions and Poisson's ratios were obtained from linear regression, in the region up to 10% compression. Only tests with a Root Mean Squared Error between the linear model and data below 0.005 were used, resulting in inclusion levels of 96% for quasi-static compressions, 82% for 0.1 m impacts and 87% for 0.2 m impacts. Comparison with manual analysis verified the accuracy of the tracking algorithm.

Footage from the impact tests was also used to identify the frames corresponding to the start and end of contact between the sample and dropper, and the maximum deformation. Aligning peak acceleration with maximum deformation allowed the start and end of contact to be identified in the acceleration-time traces. Repeated analysis of ten randomly selected impacts indicated uncertainties in contact time to be within 1 ms.

3 Results Figure 3 shows differences in the pore structures between the unconverted and converted foams. The unconverted foam and the converted foam with an LCR of 0.7 exhibit the regular open-cell and re-entrant structures, respectively, characteristic of positive Poisson's ratio and auxetic foams [10, 40]. The structure of the foam converted with an LCR of 0.85 is seen to be intermediate between the other two foams, consistent with the intermediate level of compression applied in this case.

Figure 4 shows the classical stress–strain relationship for the unconverted foam, with the start of the plateau region

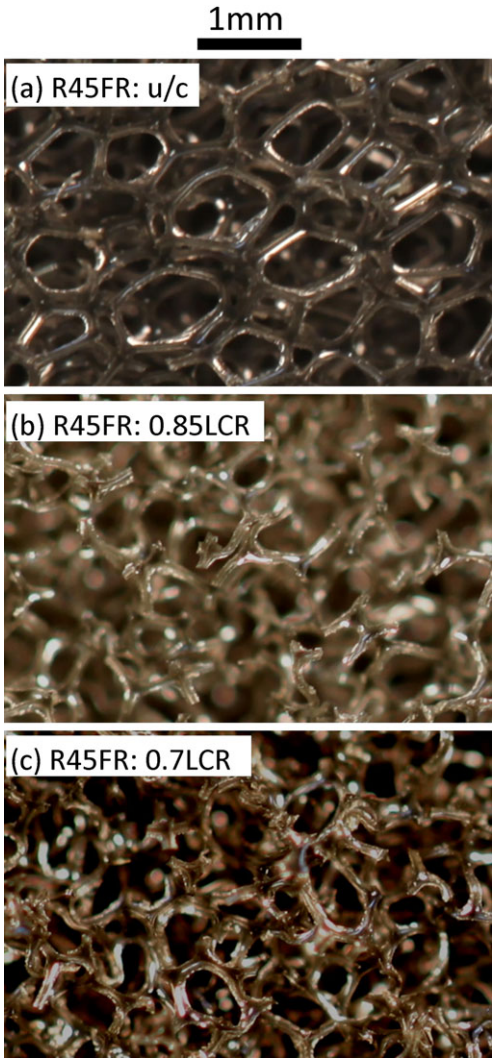

Figure 3 Through thickness images of cell structure obtained for the R45FR foams.

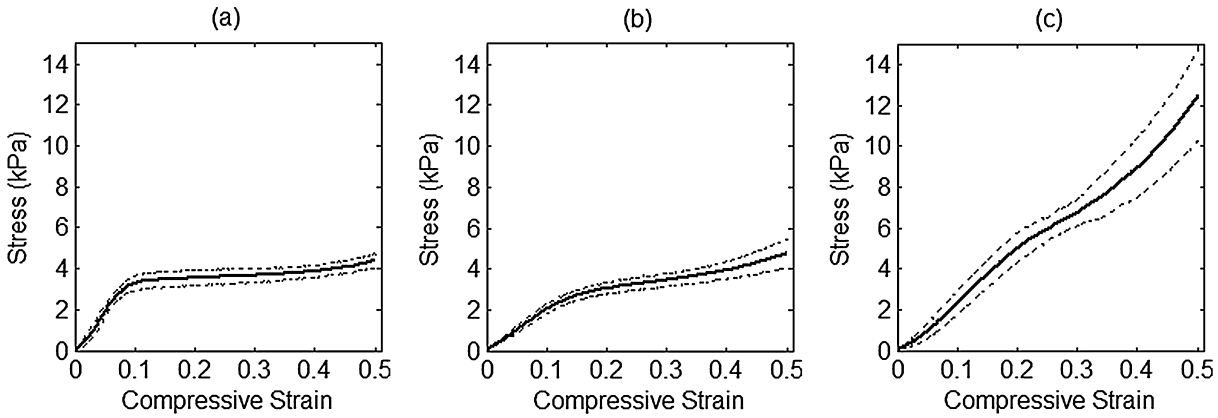

Figure 4 Mean quasi-static compressive stress–strain plots averaged across the three foam types, (a) unconverted, (b) 0.85 LCR and (c) 0.7 LCR. The dotted lines represent one standard deviation either side.

Table 2 Material properties from quasi-static and dynamic characterisation averaged across all three foam types. Values for Young's modulus and Poisson's ratio correspond to region up to 5% and 10% compression, respectively.

	Young's modulus (kPa)	Poisson's ratio		
		quasi-static	0.1 m	0.2 m
UC	35 ± 1	0.29 ± 0.20	0.24 ± 0.13	0.26 ± 0.11
0.85 LCR	20 ± 10	0.05 ± 0.12	0.04 ± 0.07	0.09 ± 0.13
0.7 LCR	18 ± 6	-0.01 ± 0.03	-0.01 ± 0.06	-0.04 ± 0.05

corresponding to cell-wall buckling occurring around 5–10% compression. The foams with the LCR of 0.7 exhibited approximately half the Young's modulus of the unconverted foam (Table 2), in agreement with Sanami et al. [8]. These re-entrant structured foams showed no significant plateau region up to maximum compression at 50% strain, indicating higher resilience. The foam with the LCR of 0.85 showed intermediate behaviour, with reduced Young's modulus in the linear region up to approximately 15% strain followed by a plateau region at higher strain.

Figure 5 shows nonlinear lateral strain-longitudinal strain relations for the unconverted foam and foams with a LCR of 0.85, with the data following a similar trend to the corresponding quasi-static stress–strain plots. The foams with a LCR of 0.7 exhibited lower lateral strain for a given longitudinal strain and did not show a significant plateau region. Table 2 confirms that Poisson's ratio decreased with LCR, with similar values obtained for each LCR from the quasi-static and impact tests. The foams with the LCR of 0.7 showed marginally auxetic behaviour, as indicated by the re-entrant pore structure and near linear quasi-static stress–strain relationship.

Figure 6 shows sample acceleration-time traces for the flat dropper impacts. For each of the foams, peak accelerations increased with impact energy. The acceleration-time traces for the unconverted foams show a dramatic increase in acceleration corresponding to the point of maximum deformation. The traces for the auxetic foams with a LCR of 0.7 had lower and less pronounced peaks, with a more gradual change in acceleration throughout impact. The foam with a LCR of 0.85 showed intermediate behaviour.

Figure 7 confirms peak accelerations for the flat-faced dropper decreased with LCR. Peak accelerations for the auxetic foams with the LCR of 0.7 were ~40% of those for the unconverted foams. Figure 8 shows contact times and times to maximum deformation for this dropper were lower when the impact energy was 4 J in comparison to 2 J. For each drop height, similar contact times were observed for the unconverted foam and foams with a LCR of 0.85.

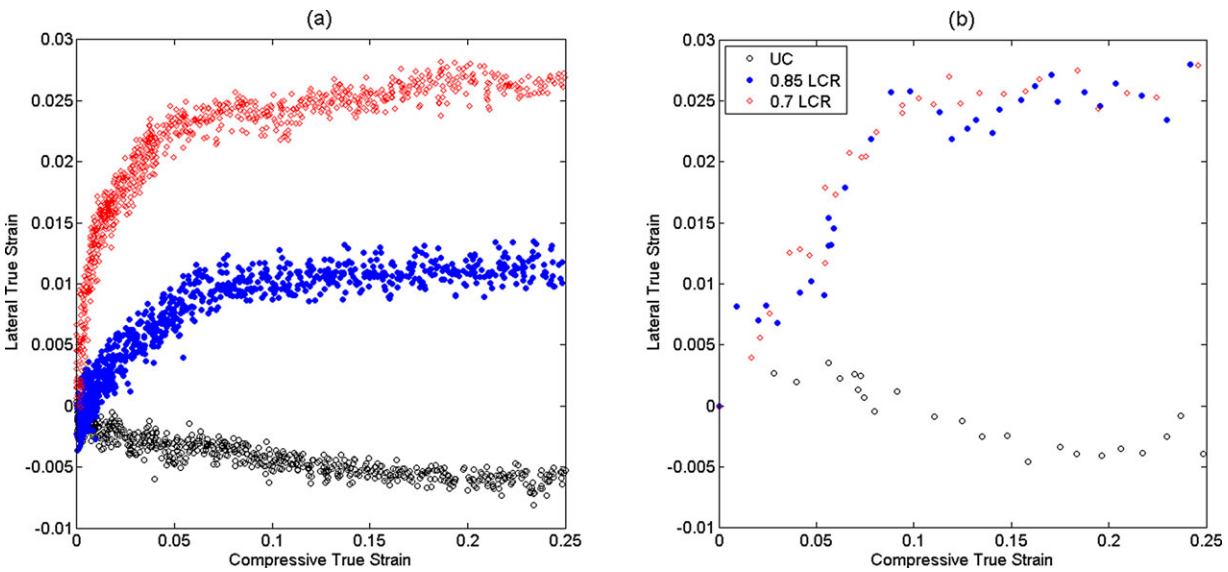

Figure 5 Sample lateral strain vs. longitudinal strain plots for R60FR foam, (a) quasi-static, Poisson's ratio at 10% true strain was −0.03 for 0.7 LCR, 0.13 for 0.85 LCR and 0.21 for UC and (b) 4 J impacts, Poisson's ratio at 10% true strain was −0.04 for 0.7 LCR, 0.24 for 0.85 LCR and 0.25 for UC.

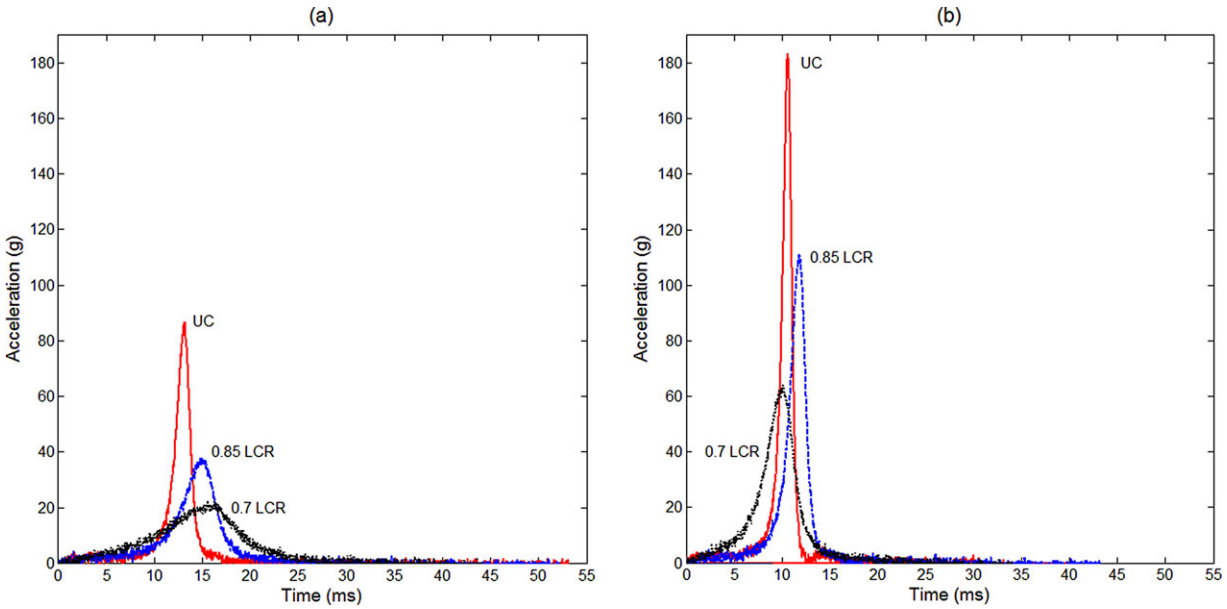

Figure 6 Sample accelerometer traces for the flat dropper on the R45FR foam, (a) 2 J and (b) 4 J. Peak acceleration was synchronised with maximum deformation from video footage and the start and end of the contact was identified from the video.

Contact times for the foams with a LCR of 0.7 were ~25% shorter than those observed for the other foams. For each drop height, times to maximum deformation were similar for all foams, indicating a shorter restitution phase for the foams with a LCR of 0.7. Assuming full deformation of the samples, the average loading rate for the impacts was in the region of 80,000–120,000 mm m^{-1}.

Figure 9 shows sample acceleration-time traces for the hemispherical dropper. The dramatic increase in acceleration at ~15 ms for the unconverted foam indicates the sample bottomed out, as confirmed in Fig. 10a. In contrast, Fig. 10c shows the auxetic sample with the LCR of 0.7 contracted laterally, densifying around the dropper and preventing bottoming out. The corresponding acceleration-time trace in Fig. 9 shows a lower and less pronounced peak with a more gradual change in acceleration throughout impact. The foam with a LCR of 0.85 showed intermediate behaviour. Figure 11 confirms peak accelerations for the hemispherical dropper decreased significantly with LCR. Peak accelerations for the auxetic foams with the LCR of 0.7 were ~80% lower than those observed for the unconverted foam.

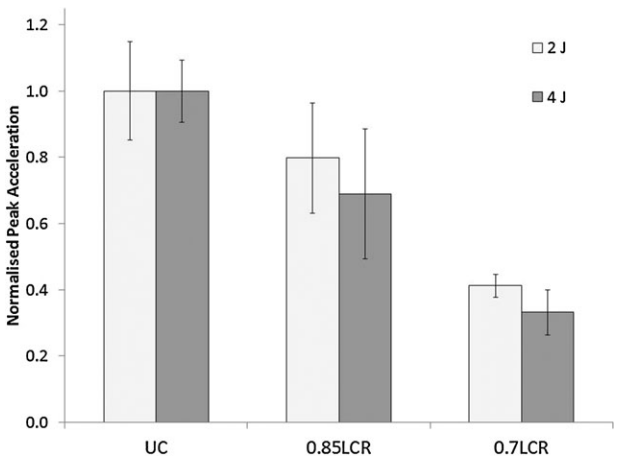

Figure 7 Flat dropper normalised peak acceleration mean for all three foams. Two joule impacts normalised to UC mean of 64 g, 4 J impacts normalised to UC mean of 182 g. Error bars correspond to one SD either side.

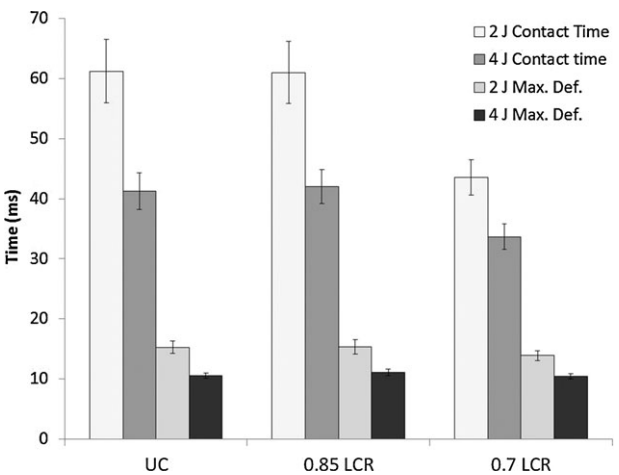

Figure 8 Flat-faced dropper contact time and time to maximum deformation averaged across the three foam types. Error bars correspond to one SD either side.

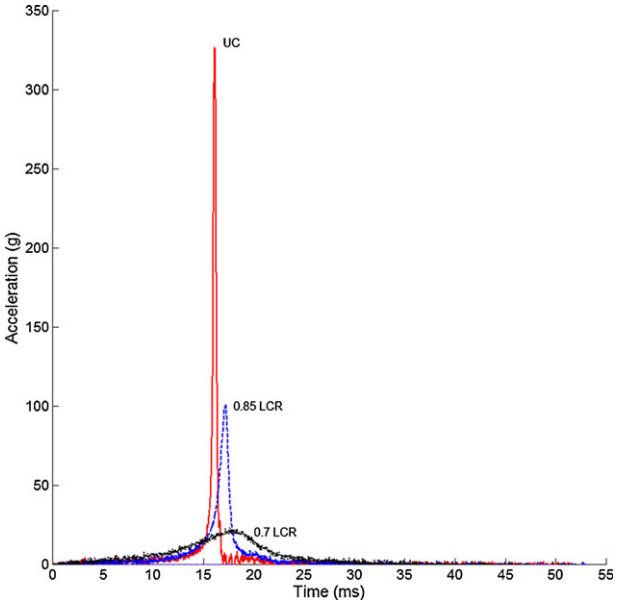

Figure 9 Sample accelerometer traces for the hemispherical dropper on the R45FR foam. Peak acceleration was synchronised with maximum deformation from video footage and the start and end of the contact was identified from the video.

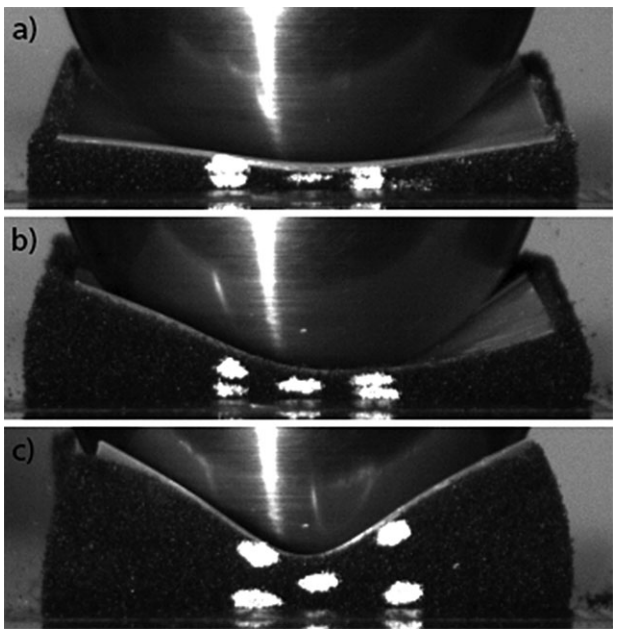

Figure 10 Maximum deformation of the hemispherical dropper on the R45FR foam, (a) unconverted at 16 ms, (b) 0.85 LCR at 17 ms and (c) 0.7 LCR at 18 ms.

4 Discussion Peak accelerations for a hemispherical dropper with 2 J of energy were ~6 times lower when impacting auxetic foams covered with a thin polypropylene sheet, in comparison to their conventional counterparts. The effect of the sheet–foam thickness ratio and the mechanical properties of the sheet, on the impact performance of the composite pads, warrants further investigation. Figure 2 clearly shows that sheet thickness can have a dramatic effect on load distribution for the underlying foam. This will be the focus of further research, along with the potential to tailor the mechanical properties of the shell. In this latter case, the ability to introduce the auxetic effect may be achieved, for example, in a carbon fibre-reinforced epoxy laminate shell [29].

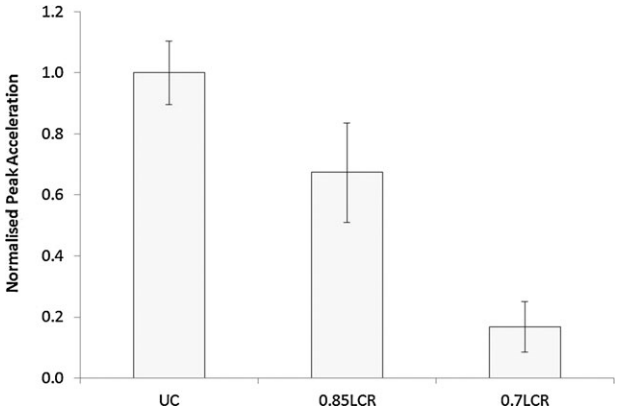

Figure 11 Hemispherical dropper normalised peak acceleration for 2 J impacts. Normalised to UC mean of 327 g. Error bars correspond to one SD either side.

For foams in isolation impacted with a flat mass with energies up to 4 J, peak accelerations were ~3 times lower for auxetic foams in comparison to the conventional foams. The significant reduction in peak accelerations for the auxetic foams was because they prevented bottoming out. No clear differences were observed in peak accelerations between levels of foam porosity in the range 30–60 pores in^{-1}.

Through thickness images and quasi-static compression testing indicated differences between conventional foams and those subjected to a thermo-mechanical conversion process. The unconverted foams exhibited classical stress–strain behaviour, with cell-wall buckling occurring at around 5–10% compression [8, 38]. Foams with a LCR of 0.7 had a re-entrant structure and stress–strain curve without a significant plateau region in agreement with Sanami et al. [8], remaining close to linear up to maximum compression at 50% strain. The auxetic foams exhibited approximately half the Young's modulus of their conventional counterparts, and the modulus values matched those reported by Sanami et al. [8].

Quasi-static and low-kinetic energy impact testing resulted in comparable values for Poisson's ratio across each of the three levels of foam conversion. Poisson ratios for the unconverted foams fell slightly below the typical value of 0.3 for polyurethane [38] and were lower than the value of 0.36 reported by Sanami et al. [8]. Negative Poisson's ratios were reported for converted foams for average loading rates up to ~120,000 mm m^{-1}. However,

Poisson's ratios for foams with a LCR of 0.7 fell only just below 0, considerably higher than the values reported in the literature for similar foams following a thermo-mechanical conversion process [8, 13, 41–43]. The Poisson's ratio of auxetic foam is likely to be a function of the conversion process – sample size and shape, LCR and conversion time and temperature – and the specific methodology for which it is measured, including the sample shape and strain range.

In this work, Poisson's ratio has been determined on very low aspect ratio (short height and large lateral dimensions) test specimens to enable investigation of strain rate. In view of the successful production of the required foam structure for auxetic behaviour, the low aspect ratio specimen geometry may be the main factor for the reduction in magnitude of Poisson's ratio compared to previous reports. Friction effects associated with the surface on which the foams are placed, and the surface of the compression plate/flat dropper, will restrict lateral movement of the foam in contact with these surfaces. For low aspect ratio specimens, edge effects due to frictional constraints at the top and bottom foam surfaces will dominate the overall lateral response of the foam. Compression testing of auxetic foam samples with different aspect ratios could help further our understanding of edge effects on the Poisson's ratio response and, therefore, the utility of auxetic foams in applications where foam thickness constraints in the design phase are significant. Further work will, nevertheless, be undertaken to optimise the conversion process with the aim of minimising Poisson's ratio.

The foundational work presented here has shown further potential for auxetic foams to be applied to protective sporting equipment. Future work will also include investigations into other base foams, focussing on their ability to be converted to auxetic foams and impact performance following conversion. Testing of these foams will also be undertaken across a wider range of impact energies and for repeated impact loading. Auxetic foam samples larger than those tested here will also need to be produced, so prototype protective sporting equipment utilising these foams can be developed and assessed against the appropriate standard.

5 Conclusions Auxetic foams have shown potential to be applied to protective sporting equipment. These foams reduced impact peak accelerations by ~6 times in comparison to their conventional counterparts, when impacted with a rigid hemisphere, the size of a cricket ball. Negative Poisson's ratios were observed for average loading rates up to ~120,000 mm m^{-1}, although the values for Poisson's ratio were not as low as those reported in the literature. Further work will aim to optimise both foam selection and the conversion process. Applying auxetic foams to protective sporting equipment while assessing performance against the appropriate testing standard is now required.

Acknowledgements We are grateful to funding received from Sheffield Hallam University via the IMAGINE project for this work. The authors would like to thank Nicolo Martinello for his assistance.

References

[1] A. C. Hergenroeder, Pediatrics **101**(6), 1057–1063 (1998).
[2] T. A. Adirim and T. L. Cheng, Sports Med. **33**(1), 75–81 (2003).
[3] R. Bahr and T. Krosshaug, Br. J. Sports Med. **39**(6), 324–329 (2005).
[4] A. McIntosh, Proc. Inst. Mech. Eng., Part P: J. Sports Eng. Technol. **226**(3-4), 193–199 (2012).
[5] S. Ankrah and N. J. Mills, Sports Eng. **6**(4), 207–219 (2003).
[6] S. Ankrah and N. J. Mills, Sports Eng. **7**(1), 41–52 (2004).
[7] N. J. Mills, in: Sport Materials, edited by M. J. Jenkins (Woodhead, Cambridge, 2003), chap. 2.
[8] M. Sanami, N. Ravirala, K. Alderson, and A. Alderson, Proc. Eng. **72**, 453–458 (2014).
[9] K. E. Evans, M. Nkansah, I. J. Hutchison, and S. C. Rogers, Nature **353**, 124 (1991).
[10] R. Lakes, Science **235**, 1038–1040 (1987).
[11] J. N. Grima, D. Attard, R. Gatt, and R. Cassar, Adv. Eng. Mater. **11**(7), 533–535 (2009).
[12] R. S. Lakes and K. Elms, J. Compos. Mater. **27**(12), 1193–1202 (1993).
[13] N. Chan and K. Evans, J. Mater. Sci. **32**(22), 5945–5953 (1997).
[14] J. B. Choi and R. S. Lakes, J. Mater. Sci. **27**, 5375–4684 (1992).
[15] A. Bezazi and F. Scarpa, Int. J. Fatigue **29**, 922–930 (2007).
[16] B. Howell, P. Prendergast, and L. Hansen, Acoustic Behaviour of Negative Poisson's Ratio Materials, DTRC–SME–91/01 (David Taylor Research Centre, Annapolis, MD, 1991).
[17] C. P. Chen and R. S. Lakes, J. Eng. Mater. Technol. **118**, 285–288 (1996).
[18] B. Moore, T. Jaglinski, D. S. Stone, and R. S. Lakes, Philos. Mag. Lett. **86**(10), 651–659 (2006).
[19] R. Lakes and K. W. Wojciechowski, Phys. Status Solidi B **245**(3), 545–551 (2008).
[20] J. N. Grima, R. Caruana-Gauci, K. W. Wojciechowski, and K. E. Evans, Smart Mater. Struct. **22**(8), 084015 (2013).
[21] A. A. Poźniak, H. Kamiński, P. Kędziora, B. Maruszewski, T. Stręk, and K. W. Wojciechowski, Rev. Adv. Mater. Sci. **23**(2), 169–174 (2010).
[22] C. Ge, J. Cell. Plast. **49**, 521–533 (2013).
[23] J. Lisiecki, T. Błazejewicz, S. Kłysz, G. Gmurczyk, P. Reymer, and G. Mikułowski, Phys. Status Solidi B **250**(10), 1988–1995 (2013).
[24] J. Lisiecki, S. Kłysz, T. Błazejewicz, G. Gmurczyk, and P. Reymer, Phys. Status Solidi B **251**(2), 314–320 (2014).
[25] T. C. Lim, A. Alderson, and K. L. Alderson, Phys. Status Solidi B **251**(2), 307–313 (2014).
[26] R. S. Lakes and A. Lowe, Cell. Polym. **19**, 157–167 (2000).
[27] F. Scarpa, J. R. Yates, L. G. Ciffo, and S. Patsias, Proc. Inst. Mech. Eng., Part C: J. Mech. Eng. Sci. **216**(12), 1153–1156 (2002).
[28] Y. Hou, R. Neville, F. Scarpa, C. Remillat, B. Gua, and M. Ruzzene, Composites B **59**, 33–42 (2014).
[29] K. L. Alderson and V. L. Coenen, Phys. Status Solidi B **245**(3), 489–496 (2008).

[30] M. Uzun, Fibres Text. East. Eur. **20**, 5(94) 70–74 (2012).
[31] K. L. Alderson, A. Fitzgerald, and K. E. Evans, J. Mater. Sci. **35**, 4039–4047 (2000).
[32] I. I. Argatov, R. Guinovart-Díaz, and F. J. Sabina, Int. J. Eng. Sci. **54**, 42–57 (2012).
[33] R. S. Lakes, Trans. ASME—J. Mech. Design **115**, 696–700 (1993).
[34] C. Kocer, D. R. McKenzie, and M. M. Bilek, Mater. Sci. Eng. A **505**, 111–115 (2009).
[35] Y.-C. Wang and R. Lakes, Int. J. Solids Struct. **39**, 4825–4838 (2002).
[36] J. Schultz, D. Griese, P. Shankar, J. D. Summers, J. Ju, and L. Thompson, in: Proceedings of the ASME 2011 International Design Engineering Technical Conferences, IDETC/CIE 2011 (August 28–31, 2011, Washington, DC), Vol. 5: 37th Design Automation Conference, pp. 955–965, doi: 10.1115/DET C2011-48000.
[37] C. Qi, S. Yang, D. Wang, and L.-J. Yang, Sci. World J. **2013**, 892781 (2013).
[38] L. L. Gibson and M. F. Ashby, Cellular Solids. Structure and Properties (Pergamon Press, Oxford, 1988), ISBN 0-08-036607-4.
[39] P. Pastorino, F. Scarpa, S. Patsias, J. R. Yates, S. J. Haake, and M. Ruzzene, Phys. Status Solidi B **244**(3), 955–965 (2007).
[40] S. A. McDonald, G. Dedreuil-Monet, Y. T. Yao, A. Alderson, and P. J. Withers, Phys. Status Solidi B **248**(1), 45–51 (2011).
[41] E. A. Friis, R. S. Lakes, and J. B. Park, J. Mater. Sci. **23**, 4406–4414 (1988).
[42] Y. C. Wang, R. S. Lakes, and A. Butenhoff, Cell. Polym. **20**, 373–385 (2001).
[43] M. Bianchi, F. L. Scarpa, and C. W. Smith, J. Mater. Sci. **43**(17), 5851–5860 (2008).